



# TOP-EVs: Technology of Protein delivery through Extracellular Vesicles is a versatile platform for intracellular protein delivery

Nazma F. Ilahibaks<sup>a,1</sup>, Arif I. Ardisasmita<sup>a,1</sup>, Songpu Xie<sup>a</sup>, Anders Gunnarsson<sup>e</sup>, Joseph Brealey<sup>f</sup>, Pieter Vader<sup>a,b</sup>, Olivier G. de Jong<sup>d</sup>, Saskia de Jager<sup>a</sup>, Niek Dekker<sup>e</sup>, Ben Peacock<sup>f</sup>, Raymond M. Schiffelers<sup>b</sup>, Joost P.G. Sluijter<sup>a,c,\*</sup>, Zhiyong Lei<sup>a,b,\*</sup>

<sup>a</sup> Laboratory of Experimental Cardiology, Department Heart & Lungs, University Medical Center Utrecht, Utrecht 3584 CX, the Netherlands

<sup>b</sup> CDL Research, University Medical Center Utrecht, Utrecht 3584 CX, the Netherlands

<sup>c</sup> Circulatory Health Laboratory, Regenerative Medicine Center, University Medical Center Utrecht, University Utrecht, Utrecht 3584 CX, the Netherlands

<sup>d</sup> Department of Pharmaceutics, Utrecht Institute of Pharmaceutical Sciences, Utrecht University, Utrecht 3584 CG, the Netherlands

<sup>e</sup> Discovery Sciences, Biopharmaceuticals R&D, AstraZeneca, Mölndal 43183, Sweden

<sup>f</sup> NanoFCM Co., Ltd, MediCity, D6 Thane Road, Nottingham NG906BH, United Kingdom

## ARTICLE INFO

### Keywords:

Extracellular vesicles  
Active protein loading  
Functional intracellular protein delivery  
Genome editing  
TOP-EV

## ABSTRACT

Extracellular vesicles (EVs) have emerged as biocompatible drug delivery vehicles due to their native ability to deliver bioactive cargo to recipient cells. However, the application of EVs as a therapeutic delivery vehicle is hampered by effective methods for endogenously loading target proteins inside EVs and unloading proteins after delivery to recipient cells. Most EV-based engineered loading methods have a limited delivery efficiency owing to their inefficient endosomal escape or cargo release from the intraluminal attachment from the EV membrane. Here, we describe the 'Technology Of Protein delivery through Extracellular Vesicles' (TOP-EVs) as a tool for efficient intracellular delivery of target proteins mediated via EVs. The vesicular stomatitis virus glycoprotein and the rapamycin-heterodimerization of the FKBP12/T82L mutant FRB proteins were both important for the effective protein delivery through TOP-EVs. We showed that TOP-EVs could efficiently deliver Cre recombinase and CRISPR/Cas9 ribonucleoprotein complex *in vitro*. Moreover, our results demonstrated that the capacity of TOP-EVs to deliver intracellular proteins in recipient cells was not an artifact of plasmid contamination or direct plasmid loading into EVs. Finally, we showed that TOP-EVs could successfully mediate intracellular protein delivery in the liver *in vivo*. Taken together, TOP-EVs are a versatile platform for efficient intracellular protein delivery *in vitro* and *in vivo*, which can be applied to advance the development of protein-based therapeutics.

## 1. Introduction

Several delivery vehicles have been developed in recent years to promote biopharmaceutical efficacy by enabling intracellular protein delivery. Currently, poor pharmacological performance by protein-based therapeutics arises from proteins' low stability, large size, hydrophilicity, and membrane impermeability [1]. To overcome these liabilities, diverse synthetic delivery vehicles, *i.e.*, lipid nanoparticles, polymers, and liposomes, have been developed with variable success for intracellular delivery of proteins *in vitro* or *in vivo* [2–4].

Extracellular vesicles (EVs) are cell-derived nanoparticles that foster

cell-to-cell communication by transferring biological cargo from their parent cell, *i.e.*, nucleic acids, proteins, and (phospho)lipids, to recipient cells. EVs encompass different sub-nanosized vesicle classes defined by their biogenesis, including exosomes (30–100 nm) microvesicles (50–1000 nm), and apoptotic bodies (>100 nm) [5,6]. EVs have a distinct biological function of altering the phenotype of their target cells [7]. EVs' biocompatibility, low immunogenicity, and intrinsic targeting abilities have increased the interest in employing them as drug delivery vehicles [8] Murphy et al. showed that these natural delivery vehicles outperform the clinically approved state-of-the-art DLin-MC3-DMA lipid nanoparticles for intracellular RNA delivery [9]. Nevertheless, strategic

\* Corresponding authors at: Laboratory of Experimental Cardiology, Department Heart & Lungs, University Medical Center Utrecht, Utrecht 3584 CX, the Netherlands.

E-mail addresses: [j.sluijter@umcutrecht.nl](mailto:j.sluijter@umcutrecht.nl) (J.P.G. Sluijter), [zlei@umcutrecht.nl](mailto:zlei@umcutrecht.nl) (Z. Lei).

<sup>1</sup> These authors contributed equally to this work.

<https://doi.org/10.1016/j.jconrel.2023.02.003>

Received 11 April 2022; Received in revised form 17 January 2023; Accepted 1 February 2023

Available online 15 February 2023

0168-3659/© 2023 The Authors. Published by Elsevier B.V. This is an open access article under the CC BY license (<http://creativecommons.org/licenses/by/4.0/>).

incorporation of target proteins inside EVs, which can be achieved through exogenous or endogenous methods, remains challenging.

Exogenous EV protein loading methods require complicated procedures to load biological payloads into isolated EVs, including electrostatic interactions, agent-induced permeabilization, sonication, electroporation, mixing, freeze-thaw cycles or extrusion [10]. Unfortunately, post-EV isolation loading methods can harm the integrity of the EVs and proteins involved, thereby altering the payload and delivery vehicle [11]. Therefore, we explored an endogenous EV protein loading method that takes advantage of cellular processes to manufacture and incorporate biotherapeutic payloads inside EVs.

Different engineering strategies have achieved significant endogenous EV loading of their target protein. However, their application for intracellular protein delivery is limited due to the covalent attachment of cargo proteins to the EV membrane or low endosomal escape. Respective of the experimental system selected, the EV-mediated cargo transfer had an efficiency of <5% in target cells *in vitro* [7,12,13]. To address these limitations, we explored the potential of rapamycin-interacting heterodimer proteins FK506-binding protein (FKBP12) and the T82L mutant FKBP12-rapamycin binding (FRB) domain [14]. FKBP12 was attached to the cellular membrane *via* the N-myristoylation sequence, and FRB was fused to target proteins through a GGSGG linker. By decorating the EVs' membrane with the fusogenic vesicular stomatitis virus glycoprotein (VSV-G), we rationalized that VSV-G will further facilitate EVs' endosomal escape in recipient cells to improve intracellular protein delivery.

Here, we developed TOP-EVs (Technology of Protein loading through Extracellular Vesicles) as a platform for efficient functional intracellular protein loading and subsequent target cell delivery. To enable a controllable and reversible target protein loading and subsequent delivery through EVs, we integrated the fusogenic VSV-G, and the rapamycin-inducible heterodimers T82L mutant FRB (DmrC) fused to a target protein with FKBP12 (DmrA) [15]. The present study demonstrated that different target proteins, including GFP, Cre, and CRISPR/Cas9 ribonucleoprotein complex (RNP), are efficiently loaded and functionally delivered *via* TOP-EVs *in vitro* to different cell types. Finally, we demonstrated that TOP-EVs could mediate the functional transfer of proteins *in vivo*. In conclusion, TOP-EVs are an attractive delivery platform to mediate intracellular protein delivery through EVs for *in vitro* and *in vivo* applications.

## 2. Methods

### 2.1. Cell culture

Human embryonic kidney 293FT (HEK293FT), HepG2 cells, human-induced pluripotent stem cell-derived fibroblast cells (iPSC-fibroblast), T47D stoptight reporter cells (provided by dr. L.Jiang [7]), and HEK293 Cas9 reporter cells [13] were grown in Dulbecco's Modified Eagle Medium (DMEM) supplemented with 10% fetal bovine serum (FBS), 1% penicillin/streptomycin (P/S). Human myoblast cells were cultured in Skeletal Muscle Cell Growth Medium (C-23160, PromoCell) supplemented with 20% FBS and 1% P/S. Human umbilical vein endothelial cells (HUVEC) were maintained in Endothelial Cell Basal Medium MV (C-22220, PromoCell) supplemented with Endothelial Cell GM MV Supplement Pack (C-39220, PromoCell) and 1% P/S. All cells were incubated in a 5% CO<sub>2</sub> environment at 37 °C. Dissociation was performed by incubating the cells with 0.25% Trypsin-EDTA solution (T4049, Sigma-Aldrich) for 3 min., or with Accutase® solution (A6964, Sigma-Aldrich) for 2 min. For HUVEC, at 37 °C and 5% CO<sub>2</sub>. All.

### 2.2. Plasmids

The TOP-EV expression cassette containing DmrC, IRES, and N-myristoylation signal(N-Myr) was subcloned into the expression vector (K65001, ThermoFisher Scientific) using the NEBuilder® HiFi DNA

assembly master mix (E2621L, NEB) according to the manufacturer's protocol. The DmrA and DmrC sequence were derived from the iDimerize™ Inducible Heterodimer System (635067, Takara Bio). Subsequently, GFP, Cre- or Cas9, was cloned at the N-terminal of DmrC with a GGSGG linker.

### 2.3. Stable cell lines

Stable GFP-TOP cell lines were created using the Flp-In™ T-Rex™ System (R78007, ThermoFisher Scientific), including the pOG44 Flp recombinase expression vector and GFP-TOP. In a gelatin-coated 6-well plate, Flp-In™ T-REx™ 293 cells were plated and incubated overnight. Following the manufacturer protocol, the pOG44 plasmid was co-transfected with GFP-TOP expression construct (9:1 ratio, w:w) with Lipofectamine® 3000 Transfection Reagent (L3000008, Invitrogen). Cells were split the next day at approximately 25% confluency and incubated with 200 µg/µl hygromycin B gold (ant-hg-1, Invivogen). When individual foci could be identified, resistant colonies were harvested, expanded, and subsequently cultured according to the standard culturing protocol for HEK293 cells in the presence of hygromycin.

### 2.4. GFP-TOP time-lapse experiment

For the GFP TOP time-lapse experiment, µ-Slide 8 well-chambered coverslips (80,827, ibidi) were coated with 0.1% gelatin. Per well, 100,000 GFP TOP Flp-In™ T-REx™ 293 cells were seeded the day before doxycycline (1 µg/ml) treatment. Prior to imaging, NucBlue™ live cell stain (R37605, Life Technologies) was added according to the manufacturer's protocol. The microscope slide was kept at 37 °C and 5% CO<sub>2</sub>. Locations of cells were set with the DeltaVision™ ultramicroscope with 60× magnification. Subsequently, 500 nM A/C heterodimerizer ligand (635055, Takara Bio) was added per well. All selected locations were checked and corrected. The interval was set at 5 min. For 12 h.

### 2.5. Ligands-induced GFP membrane translocation

GFP-TOP cells were seeded in a 24-well plate containing 12 mm PEI coated cover glasses (25 × 103 cells/well) and incubated overnight. Cells were cultured with 1 µg/ml doxycycline and A / C heterodimer ligand (635,055, Takara Bio), i.e., with 0, 250, or 500 nM. After 24 h, the cells were washed with PBS and incubated with a standard growth medium. After 2 h, cells were fixed with 4% PFA and mounted on microscopy glasses with Fluoromount-G (0100-01, SouthernBiotech). Microscopy analysis was performed with the EVOS FL Cell Imaging System (LifeTechnologies) and the LSM 700 confocal microscopy (Zeiss).

### 2.6. TOP-EV production and purification

$1 \times 10^7$  HEK293FT cells were seeded in T175 flasks and cultured overnight. The following day, for GFP and Cre TOP-EV production, T175 flasks of HEK293FT cells were transfected with GFP-TOP or Cre-TOP plasmid (30 µg) and VSV-G (15 µg) in a 1:2 DNA:Lipid (w:w) ratio with Lipofectamine® 3000 Transfection Reagent (L3000008, Invitrogen Corp.), following manufacturer's protocol. Similarly, Cas9 TOP-EVs were produced by transfecting a T175 flask with Cas9-TOP plasmid (15 µg), sgRNA (15 µg), and VSV-G (15 µg) plasmid. After 6 h after transfection, the medium was changed to DMEM supplemented with 10% exosome-depleted FBS (A2720801, Gibco), 1% P / S and 500 nM of A / C heterodimerizer (635,055, Takara Bio). After 72 h, the conditioned medium was isolated and centrifuged at 2000 xg for 15 min., at 4 °C. Next, TOP-EVs were obtained from the conditional medium by differential centrifugation using a 38.5 ml, open top thinwall polypropylene tube (326,823, Beckman Coulter) and SW 32 Ti swinging bracket (369,694, Beckman Coulter). The supernatant was centrifuged at 10,000 xg for 30 min at 4 °C. Finally, the supernatant was centrifuged at 100,000 xg for 60 min. at 4 °C to pellet the vesicles. The TOP-EV pellet

was recovered by suspending the pellet in PBS and filtered through a 0.45 µm syringe SFCA membrane filter (516–1954, Corning).

## 2.7. Cre and CRISPR/Cas9 reporter assays

In a 96-well flat-bottom plate (655075, Greiner CELLSTAR), T47D stoplight reporter or HEK293 Cas9 stoplight reporter cells were seeded at a density of 10,000 cells/well and incubated overnight. After 24 h, TOP-EV were added to the medium. After 72 h, unless stated otherwise, the cells were directly visualized with EVOS Cell Imaging System (M5000, Invitrogen) and subsequently analyzed by flow cytometry (CytoFLEX, Beckman Coulter).

## 2.8. Cre TOP-EV uptake inhibitor assay

In a 96-well plate (655,075, Greiner CELLSTAR), 10,000 T47D stoplight reporter/well were seeded and incubated overnight. Prior to TOP-EV addition, cells were incubated with nystatin (20 µg/ml, N6261, Sigma-Aldrich), chlorpromazine (40 µM, C0982, Sigma-Aldrich), ethylisopropylamiloride (EIPA) (30 µM, A3085, Sigma-Aldrich), or chloroquine (40 µM, C6628, Sigma-Aldrich) for 30 min. Next,  $1.22 \times 10^9$  particles of Cre TOP-EVs were added to the medium and incubated with inhibitors for 4 h. Subsequently, the medium was aspirated, cells were washed with PBS, and fresh medium was added. After 48 h, cells were imaged EVOS FL Cell Imaging System (LifeTechnologies) followed by flow cytometric analysis.

## 2.9. Plasmids contamination analysis using dox-inducible Wildtype GFP and TOP-EV GFP constructs

Doxycycline-inducible GFP plasmid as well TOP-EV GFP plasmids were transfected with or without VSV-G plasmid per flask in a DNA:Lipid 1:2 (w:w) ratio with Lipofectamine 3000 Reagent (L3000008, Invitrogen Corp.) in HEK293FT cells, following manufacturer's protocol. After 72 h, the conditioned medium was isolated, and EVs were purified with differential ultracentrifugation. GFP EVs and GFP TOP-EV ( $1 \times 10^{10}$  number of particles) were combined with DMEM supplemented with 10% FBS, 1% P/S with or without doxycycline to recipient HEK293FT cells in a 96-well flat-bottom plate (655,075, Greiner Bio). After 24 h, the donor and target cells were imaged EVOS FL Cell Imaging System (LifeTechnologies).

## 2.10. Nanoparticle tracking analysis

The size and particle concentration of EVs were assessed with nanoparticle tracking analysis (NTA) equipped with a 405 nm laser (Malvern Nanosight NS500). EVs were dispersed in PBS that gave between 30 and 100 tracks per frame. Samples were measured in triplicate with individual measurements of 30 s at camera level 15. Analysis was performed with NTA software 3.3 with a minimal track length of 10, detection threshold 5, and screen gain 1. Cut-off values for reliable measurement were between 20.0 and 100.0 particles/frame.

## 2.11. Flow cytometry analysis

For flow cytometry measurements, the cells were washed with PBS and dissociated with 0.25% Trypsin-EDTA solution (Sigma-Aldrich, T4049). Subsequently, the cells were collected in a 96-well round bottom plate (650,185, Greiner CELLSTAR®) by centrifugation at 500 xg for 3 min. and were resuspended in 250 µl PBS + 2% FBS. The cells were analyzed by CytoFLEX (Beckman Coulter) and further analyzed by Kaluza software v2.1 (Beckman Coulter Inc.).

## 2.12. T7E1

DNA was obtained according to the manufacturer's instructions of

the GeneJET Genomic DNA Purification Kit (K0721, Thermo Scientific). Genomic DNA was PCR amplified using Q5® Hot Start High-Fidelity 2× Mastermix (M0494L, NEB), Fw: 5'-GACATCACCTCCACAACGA-3' and Rev.: 5'-CTTCAGCTCGATGCGGTTCA-3'. The PCR product was denatured and reannealed using a thermocycler together with NEBuffer 2.1 Buffer following the manufacturer's instructions. Next, 1 µL of T7 Endonuclease (T7E1, NEB) was added and incubated at 37 °C for 1 h. The products were loaded on a 2% Agarose TAE gel and analyzed using Chemi Doc™ XRS + system (Bio-Rad) and Image Lab™ software.

## 2.13. Transmission electron microscopy (TEM)

Cre TOP-EVs and Cas9 TOP-EVs containing VSV-G were produced via transiently transfected HEK293FT donor cells cultured in the presence of the ligand. The TOP-EVs were obtained via differential ultracentrifugation and suspended in PBS. The TOP-EVs were adsorbed to carbon-coated grids (75–200 mesh) for 15 min. at room temperature. Subsequently, the grids were washed with PBS, fixated with 2% PFA, and 0.2% glutaraldehyde in PBS for 30 min. at room temperature. Next, uranyl-oxalate was used for staining, and the grids were embedded with 1.8% methylcellulose and 0.4% uranyl acetate for 10 min. on ice. TOP-EVs were visualized with a JEOL 3 microscope.

## 2.14. Western blot

TOP-EVs were lysed using RIPA lysis buffer (20–188, Merck) on ice. Samples were centrifugated at 14000 x g for 10 min. at 4 °C and the supernatants were isolated. Protein concentrations were measured using Micro BCA Protein Assay Kit (23,235, Thermo Fisher Scientific) according to the manufacturer's instructions. Lysates were mixed with NuPAGE LDS Sample Buffer (NP0007, Invitrogen) and NuPAGE Sample Reducing Agent (NP0009, Invitrogen), incubated for 10 min. at 70 °C, and then loaded into Bolt 4–12% Bis-Tris Plus Gels (NW04120BOX, Invitrogen). Electrophoresis was performed using NuPAGE MOPS SDS Running Buffer (NP000102, Invitrogen) for 32 min. at 200 V. Proteins were then transferred to iBlot PVDF membranes (IB24002, Invitrogen) and subsequently blocked with 5% BSA in TBS for 1 h at room temperature. Afterward, membranes were incubated with primary antibodies overnight at 4 °C. Primary antibodies used were as follows: mouse anti-Cre recombinase (1:1000, MAB3120, clone 2D8, Millipore), mouse anti-Alix (1:1000, ab117600, clone 3A9, Abcam), mouse anti-β Actin (1:5000, A5441, clone AC-15, Sigma-Aldrich), rabbit anti-calnexin (1:500, GTX101676, GeneTex), mouse anti-CD9 (1:1000, sc-13,118, C-4, Stata Cruz Biotechnology), mouse anti-Syntenin (1:500, TA504796, Origene), rabbit anti-VSV-G epitope tag (1:5000, NB100–2485, Novus Biologicals), rabbit anti-GFP (1:1000, 2956S, clone D5.1, Cell Signaling), and mouse anti-Cas9 (1:500, NBP2–36440, clone 7A9-3A3, Cell Signaling). Next, the membranes were washed and incubated with secondary antibodies for 1 h at 24 °C. Secondary antibodies used were goat anti-rabbit (1:2000, P0448, Dako) or goat anti-mouse (1:2000, P0447, Dako). The proteins were detected using Western-Ready ECL Substrate (426,303, Biolegend) using Chemi Doc™ XRS + system (Bio-Rad) and Image Lab™ software.

## 2.15. Single-molecule localization microscopy

GFP TOP-EVs (–/+; Ligand/VSV-G) and (+/+; Ligand/VSV-G) were serially diluted in PBS and adjusted to the same particle count, as determined by NTA before being sedimented on microscopy-compatible 384-well glass plates (Cellvis). Samples were imaged at multiple dilutions using a 60× oil immersion objective (NA = 1.49) mounted on a Ti Eclipse inverted microscope (Nikon), equipped with a FITC filter cube for GFP fluorescence imaging, CoolLED pE4000 illumination system (490 nm illumination) and an Orca Flash 4.0 CMOS camera (Hamamatsu). Multiple images (200 × 200 µm<sup>2</sup>) were acquired per sample using identical illumination and focus (via Perfect Focus System).

Analyzed images had an EV density of  $<1\text{EV}/10\ \mu\text{m}^2$  to avoid particle overlap and  $50 \times 50\ \mu\text{m}^2$  regions cropped at the center of the image to minimize the effect of vignetting and uneven illumination. EVs were detected as diffraction-limited objects corresponding to the point spread function of the microscope, confirming the detection of individual vesicles. Particle identification and quantification of peak intensity (ImageJ) were made using a threshold image ( $>2$ -fold background intensity). Detected spots with areas below  $0.1\ \mu\text{m}^2$  and above  $10\ \mu\text{m}^2$  were removed to filter out the noise and larger aggregates. For the determination of the single-molecule GFP copy number, recombinant GFP (rGFP; SinoBiological) was used as the reference fluorophore. Briefly, rGFP was added to empty wells in 10-fold dilutions (from 1 nM) and multiple dilutions were imaged using identical settings as above. The identification and quantification of the peak intensity (ImageJ) of individual fluorophores was achieved using a threshold image ( $>2$ -fold background intensity). Subsequent time-resolved imaging of the individual fluorophores was used to confirm the signal originated from single fluorophores, by recording the bleaching traces. Any object that showed multistep bleaching traces was removed from the analysis. The resulting intensity histogram was used to estimate the average signal of individual fluorophores. Similarly, the intensity histogram of the EVs was used to estimate the average signal and, by directly dividing by the fluorophore intensity, the absolute protein copy number could be estimated. Due to the high heterogeneity and lower purity of the EV samples compared to recombinant GFP samples, a more stringent threshold of three GFP molecules was defined as the detection limit of SMLM to provide a more robust analysis.

## 2.16. Nano-Flowcytometry

Prior to Nano-Flow Cytometry analysis, GFP TOP-EVs (–/+; Ligand/VSV-G) and (+/+; Ligand/VSV-G) were serially diluted in PBS and adjusted to the same particle count as determined by NTA. Samples were measured using the Flow NanoAnalyser to determine size and concentration, then stained for tetraspanins and membrane. For Tetraspanin staining, a cocktail of APC-conjugated anti-CD9, CD63, and CD81 antibodies was used. For membrane staining, MemGlow 640 was used. EVs were diluted to  $2 \times 10^{10}$  particles/ml in PBS.  $9\ \mu\text{L}$  was incubated with the antibody cocktail at 1:200 dilution, or 1:1000 for MemGlow 640. This mixture was incubated at room temperature for 30 min. in the dark, then diluted 1 in 100 in TE buffer and measured using the Flow NanoAnalyser.

A NanoAnalyzer U30 instrument (NanoFCM Inc.) equipped with dual 488/640 nm lasers was used for the simultaneous detection of side scatter (SSC) and fluorescence of individual particles. Single-photon counting avalanche photodiode detections (SPCM APDs) with band-pass filters allowed for collection of light in specific channels (SSC - 488/10; FL1–525/40; FL2–670/30). Gravity fed HPLC-grade water served as the sheath-fluid, sampling pressure by air pump module was 1 kPa, and measurements were taken over 1-min. All samples were diluted to attain a particle count within the optimal range of 2000–12,000/min.

Particle concentrations were determined by comparison to a standard containing 250 nm silica nanoparticles of known concentration to calibrate the sample flow rate. EV isolates were sized according to standard operating procedures using a proprietary 4-modal silica nanosphere cocktail (NanoFCM Inc., S16M-Exo). Using the NanoFCM software (NanoFCM Profession V2.0), a standard curve was generated based on the intensity of side scattered light of the four different silica particle populations of 68, 91, 113 and 155 nm in diameter. The laser was set to 15 mW and 10% SSC decay.

Additional fluorescent labeling of EVs was performed with MemGlow 640 and a cocktail of APC-conjugated anti-CD9 (MEM-61, Ab82389, Abcam), -CD63 (MEM-259, A15712, Thermo Fisher), and -CD81 (M38, ab233259, Abcam) antibodies.  $9\ \mu\text{L}$  of the sample, diluted to  $2 \times 10^{10}$  particles/ml in PBS, was mixed with  $1\ \mu\text{L}$  of the label, before incubation for 30 min at room temperature. The incubation

concentration ratio was 1:200 for the antibody cocktail ( $1\ \mu\text{L}$  of 1:20 antibody cocktail in PBS) and 1:1000 for MemGlow 640 ( $1\ \mu\text{L}$  of 1:100 MemGlow 640). After incubation, the mixture was diluted 1:100 in TE buffer to  $1 \times 10^8$ – $1 \times 10^9$  particles/ml for immediate phenotypic analysis.

Data processing was handled within the nFCM Professional Suite v2.0 software, with dot plots, histograms, and statistical data provided in a single PDF. Gating within the software allows for proportional analysis of subpopulations separated by fluorescent intensities with size distribution and concentration available for each subpopulation.

## 2.17. Animals

Animal care and handling were carried out with the approval of the Animal Ethical Experimentation Committee of Utrecht University, The Netherlands. As well as per the guidelines of the “Guide for the Care and Use of Laboratory Animals under work protocol no.105151.” B6.Cg-Gt (ROSA)26Sortm9(CAG-tdTomato)Hze/J transgenic mice (Ai9 mice, strain #007909), obtained from The Jackson Laboratory, were kept in our local breeding facility. The Ai9 mice were housed under standard conditions, i.e., standard chow diet with 12 h light/dark cycles.  $10^{12}$ /ml Cre TOP-EV was administered by tail vein injection ( $100\ \mu\text{L}$ ). After 5 days, mice were sacrificed and analyzed for tdTomato expression.

## 2.18. Intravenous administration of Cre EVs

The Ai9 mice were divided between a control group ( $n = 3$ ) and a group that received multiple injections of Cre -EVs ( $n = 3$ ). Via intravenous injection,  $5 \times 10^{11}$  number of particles of Cre EVs were administered within a 24-h interval for a duration of 3 days. As a negative control, Ai9 mice were injected with  $100\ \mu\text{L}$  PBS. After 7 days, the mice were sacrificed.

## 2.19. Immunofluorescence staining

The tissues had been routinely fixed in formalin for 24 h and embedded in paraffin. The paraffin-embedded organs were cut into  $5\ \mu\text{m}$  sections, fixed on slides, and dried at  $55\ ^\circ\text{C}$  for 1 h. Sections were deparaffinized and rehydrated ( $3 \times$  Tissue Clear 5 min.,  $2 \times$  99% EtOH for 5 min.,  $2 \times$  96% EtOH for 5 min.,  $2 \times$  70% EtOH for 5 min.,  $3 \times$  demi water for 5 min.). Next, the antigen retrieval was performed by submerging the slides in sodium citrate (pH = 6.0) with 0.5% Tween20 and cooking in the autoclave. The slides were washed in PBS ( $3 \times 5$  min.) and blocked with 3% BSA for 1 h at room temperature. The tdTomato+ positive cells were stained with primary antibody RFP Antibody Pre-adsorbed (1:250, Rockland Immunochemicals Inc.) followed by the secondary antibody Goat anti-Rabbit IgG (H + L) Cross-Adsorbed Secondary Antibody, Alexa Fluor 555 (1:200, A-21428, Invitrogen). Nuclei were stained with Hoechst (1:10,000, H3570, Invitrogen). The slides were covered with Fluoromount-G (0100–01, SouthernBiotech). Tissue sections images were captured with a BX53 microscope (Olympus).

For co-staining with a hepatocyte marker, following antigen retrieval, tissue slices were blocked with 5% BSA for 1 h at room temperature. Tissue sections were incubated with HNF4A (1:1000, HPA004712, Atlas Antibodies) and RFP antibody (AB1140–100, Origene) in 1% BSA in PBS overnight at  $4\ ^\circ\text{C}$ . Subsequently, tissue sections were washed with PBS ( $3 \times 5$  min.) and incubated for 1 h at room temperature with secondary antibody conjugated to Alexa 568 conjugate ( $5\ \mu\text{g}/\text{mL}$ , A11057, ThermoFisher Scientific) and secondary antibody conjugated to Alexa 488 conjugate ( $5\ \mu\text{g}/\text{mL}$ , A21206, ThermoFisher Scientific). Next, tissue sections were washed in PBS ( $3 \times 5$  min.) and incubated with Hoechst ( $0.1\ \mu\text{g}/\text{mL}$ , Invitrogen, H3570) for 15 min. at room temperature. Afterward, sections were washed with PBS ( $3 \times 5$  min.) and mounted using Mowiol (9002-89-5, Merck). Tissue section images were visualized with a Leica Tunder.



## 2.20. Statistical analysis

The statistical analysis was carried out using GraphPad PRISM v.9.3. Comparisons between two groups were analyzed using an unpaired *t*-test as indicated. One-way ANOVA analyzed comparisons between multiple groups with Tukey's multiple comparison post-test. Data is represented as mean  $\pm$  SEM with *p*-values \* < 0,05 and \*\* < 0,01 were considered statistically significant.

## 3. Results

### 3.1. Ligand-induced dimerization of DmrA and DmrC promote GFP active loading into EVs

To validate our approach and the reversible interaction between DmrA and DmrC (Fig. 1A), we used a GFP-TOP stable cell line and exposed it to the rapamycin-ortholog (ligand). After 24 h incubation with the rapamycin orthologue (ligand), confocal microscopy confirmed GFP translocation out of the nucleus (Fig. 1B).

Next, we explored whether this approach could lead to an effective loading of GFP within EVs. TOP-EVs were generated by transient transfection of HEK293FT with the GFP TOP-EV plasmid, with or without VSV-G co-transfection. Afterward, the donor cells were cultured with exosome-depleted media and EVs were isolated via differential ultracentrifugation (Fig. 1C). The relative amount of GFP protein in the isolated EVs was determined via western blot analysis and using Alix as EV protein marker (Fig. 1D). Co-culturing the donor cells with the ligand did not significantly increase without the presence of VSV-G (Fig. 1E). However, GFP loading within EVs increased when the donor cells were co-transfected with VSV-G and co-cultured with the ligand.

The GFP cargo loading efficiency was further investigated using Nano Flow analysis and single-molecule localization microscopy analysis (Fig. S2) [15,16]. Consistent with the findings of the western blot analysis, we observed the percentage of GFP positive TOP-EVs (+/+; Ligand/VSV-G) to be the highest compared to other GFP TOP-EV groups (Fig. S2). Additionally, the number of GFP molecules inside a single TOP-EV (+/+; Ligand/VSV-G) was also higher compared to the other TOP-EV groups (Fig. S3). Accordingly, TOP-EVs (+/+; Ligand/VSV-G) could mediate the intracellular delivery of GFP inside HEK293FT as determined by microscopy analysis (Fig. 1F). GFP TOP-EVs containing tetraspanins ranged from 11.3% (-/+; Ligand/VSV-G) to 18.6% (+/+; Ligand/VSV-G), which indicated that a large portion of VSV-G EVs don't express tetraspanins. Our findings from GFP TOP-EVs showed that the VSV-G and ligand inducible interaction between DmrA and DmrC are fundamental to promote endogenous protein loading and delivery through TOP-EVs.

### 3.2. TOP-EV mediate intracellular protein delivery is not mediated by the plasmid carryover

Since TOP-EVs were produced from transiently transfected from HEK293FT cells, we explored the possibility of plasmid DNA carryover either during TOP-EV production or through direct loading into EVs during EV biogenesis. To prove that TOP-EV delivery capability results from direct intracellular protein delivery and not plasmid contamination, we used doxycycline (dox)-inducible GFP construct. In the presence of dox, the transgene expression is facilitated by the expression of the TRE3G transactivator in the construct. (Fig. 2A). If TOP-EVs transfer the dox-inducible GFP construct to recipient cells, GFP expression would be observed in the recipient cells cultured with dox and *vice versa* (Fig. 2B). GFP TOP-EVs and dox-inducible GFP EVs were produced as aforementioned and administrated to the recipient HEK293FT cells cultured with or without dox. After 24 h, the presence of GFP was only observed in GFP TOP-EV treated recipient cells cultured with or without dox (Fig. 2C). No GFP was detected in the recipient cells cultured with dox and treated with EVs from cells transfected with the dox-inducible

GFP construct (Fig. 2C). This result consolidated our concept that TOP-EVs could facilitate protein delivery not due to plasmid contamination during isolation or direct loading of the plasmid into EVs.

### 3.3. Production and characterization of Cre TOP-EV

Since TOP-EVs successfully delivered GFP to recipient cells, we investigated whether Cre recombinase could be effectively loaded and unloaded through TOP-EVs. TOP-EVs were generated by transient transfection of HEK293FT with the Cre TOP plasmid with or without VSV-G co-transfection. After 72 h incubation, TOP-EVs were isolated from the supernatant by differential ultracentrifugation. Nanoparticle Tracking Analysis (NTA) demonstrated a similar size distribution between groups, co-transfected with or without VSV-G, with a mean size of  $110,3 \pm 1,64$  nm and  $108,9 \pm 1,94$  nm, respectively (Fig. 3A and B). Furthermore, EVs' without or with VSV-G had a mode size of  $84,3 \pm 3,8$  nm and  $82,0 \pm 4,2$  nm, respectively. As previously reported [17], the introduction of VSV-G increased the number of particles/ml obtained after TOP-EV isolation by 3-fold compared to the donor cells without VSV-G (Fig. 3C). TEM images from TOP-EVs obtained from donor cells co-transfected with VSV-G displayed cup-shaped morphologies with an approximate size of 100 nm (Fig. 3D). Next, we determined the relative amount of Cre protein level in the isolated EVs via western blot analysis normalized by Alix as EV protein marker (Fig. 3E and F). TOP-EVs carried 2.1-fold more Cre proteins when donor cells were cultured in the presence of the ligand (Fig. 2F). Furthermore, co-transfection of VSV-G and co-culturing the donor cells with the ligand increased Cre protein loading by 2.8-fold relative to TOP-EVs obtained without these conditions. Our findings from Cre TOP-EVs confirmed that the VSV-G and ligand-inducible interaction between DmrA and DmrC are both fundamental to improve endogenous protein loading inside TOP-EVs.

### 3.4. Functional TOP-EV mediated protein delivery in vitro

To confirm whether TOP-EV loading will lead to functional protein delivery in target cells, we used a Cre-LoxP-based T47D stoplight reporter system [18]. Successful TOP-EV mediated intracellular delivery of Cre recombinase into the Cre-LoxP-based target cells will result in recombination and color-switch from a DsRed+ signal to recombined GFP+ reporter cells (Fig. 3G). Cre TOP-EVs were isolated from transiently transfected HEK293FT cells, co-transfected with or without VSV-G and cultured with or without the ligand. The administration of Cre EVs (+/+; Ligand/VSV-G) mediated functional Cre delivery leading to  $96,1 \pm 2\%$  recombined eGFP+ reporter cells as determined by microscopy and flow cytometry analysis (Fig. 3H and I). These findings demonstrated the importance of both DmrA/DmrC and VSV-G for endogenous protein loading and successful TOP-EV mediated intracellular protein delivery.

To study the dose- and time-dependent effects of TOP-EV administration, different concentrations of TOP-EVs were administered to T47D reporter cells and TOP-EV mediated Cre recombination in T47D stoplight reporter cells was studied over time. The administration of  $2 \times 10^9$  Cre TOP-EVs (+/+; Ligand/VSV-G) to T47D stoplight reporter cells demonstrated that the percentage of GFP+ reporter cells reached a plateau at 240 min post-administration (Fig. 4A). Furthermore, increasing Cre TOP-EVs (+/+; Ligand/VSV-G) doses to T47D stoplight reporter cells demonstrated that a maximal percentage of recombined GFP+ reporter cells reached maximal recombination after the administration of  $1 \times 10^{10}$  number of particles (Fig. 4A). These observations indicate that Cre TOP-EVs' uptake is dose- and time-dependent whereby the administration of  $1 \times 10^{10}$  particles was sufficient to obtain a stable recombination 240 min post-administration.

We subsequently assessed TOP-EVs' (+/+; Ligand/VSV-G) ability to mediate functional Cre delivery in various cell types with the Cre-LoxP-based reporter system [18]. The administration of Cre TOP-EVs (+/+; Ligand/VSV-G) delivery resulted in highly efficient Cre-mediated

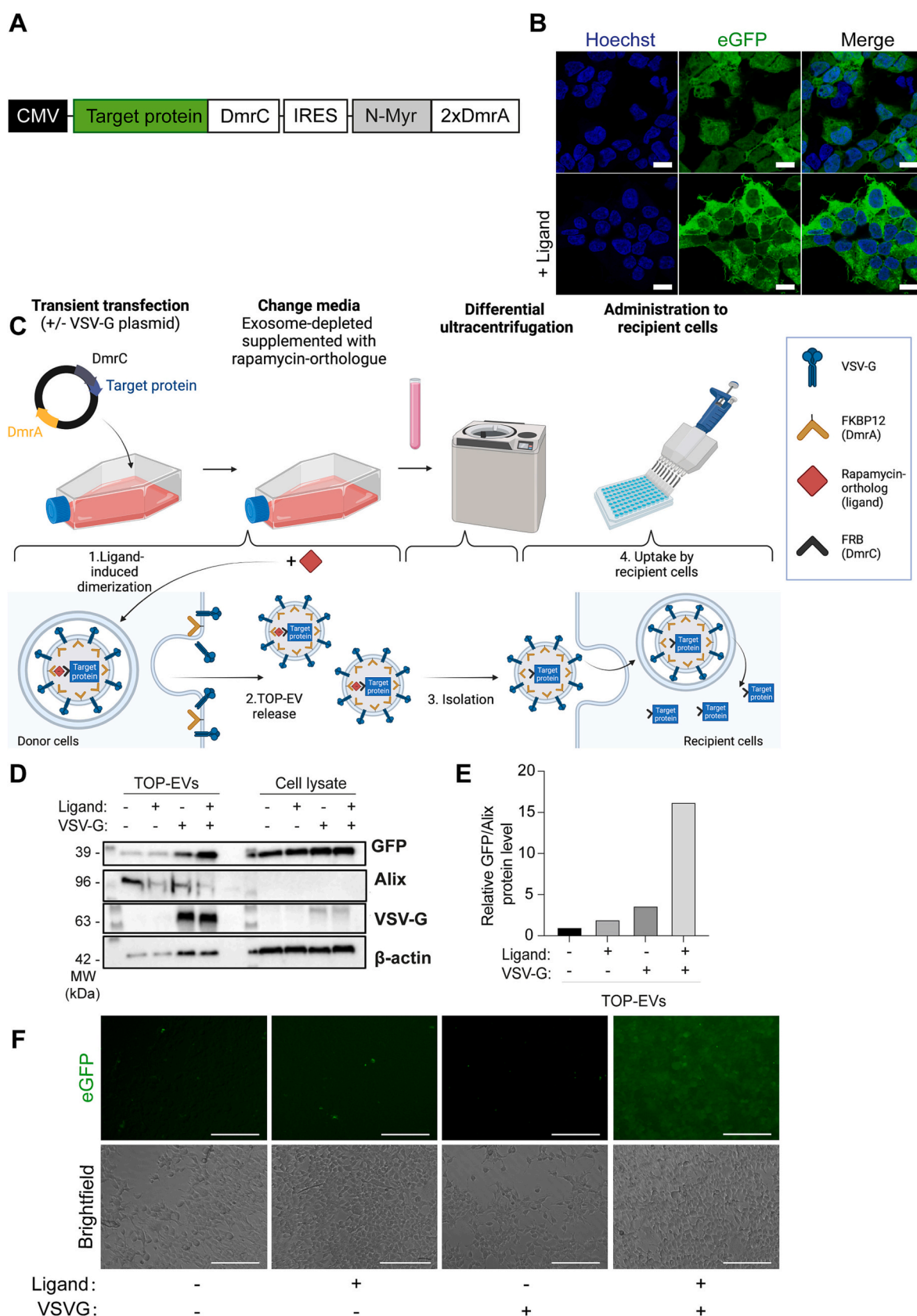


**Fig. 1. GFP delivery via Technology of Protein delivery through Extracellular Vesicles** A. Schematic illustration of the TOP-EV construct used for TOP-EV production. B. Confocal images show GFP-DmrC translocation to the membrane in the presence of the ligand. Scale bar = 15  $\mu$ m. C. Schematic illustration of TOP-EV production through transient transfection followed by differential ultracentrifugation to isolate the TOP-EVs. D. Validation of GFP expression in the producing cell and enrichment of GFP in the EVs by western blot. E. Quantification of western blot analysis of GFP enrichment in the EVs normalized by the amount of Alix in each sample. F. Uptake of GFP TOP-EV in HEK293FT cells at indicated producing condition. Scale bar = 200  $\mu$ m.

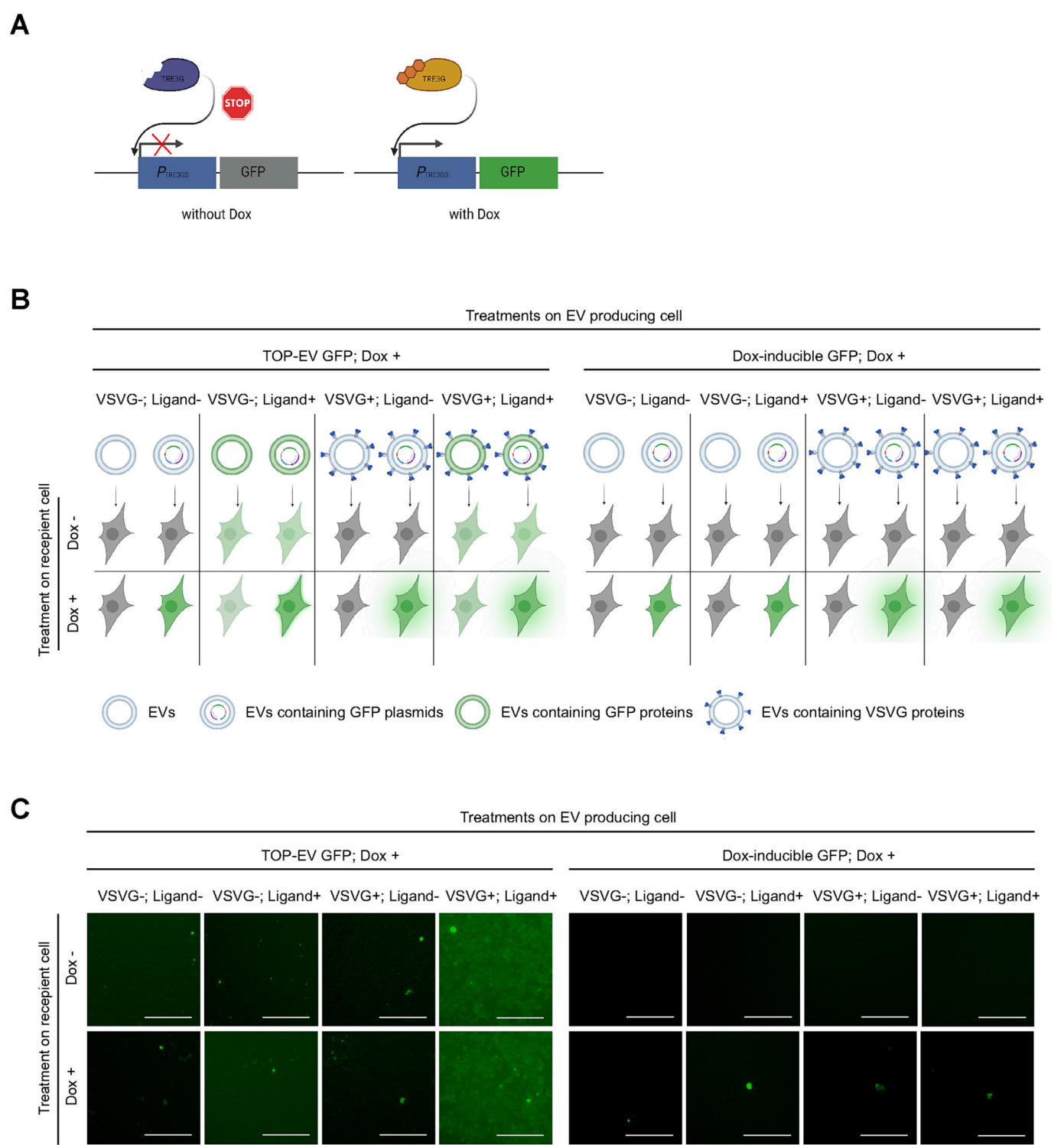


**Fig. 2. TOP-EV-mediated GFP protein transfer is not caused by plasmid carry-over.** A. Schematic illustration showing the mechanism of dox-inducible GFP expression. GFP proteins are only expressed in the presence of dox due to the activation of TRE3G transactivator proteins. B. A schematic illustration depicting the experimental design. As indicated, 8 different EVs were prepared and administrated to HEK293FT recipient cells in the presence or absence of dox. If there is plasmid contamination, GFP expression will be detected in all dox treated recipient cells. If there is no plasmid contamination, GFP expression will not change in the recipient cells regardless of dox treatment. C. Microscopy images of GFP expression after incubation of  $1 \times 10^{10}$  GFP TOP-EVs or dox-inducible GFP EVs in HEK293FT cells. GFP is only detected in the cells treated with TOP-EV produced from donor cells co-transfected with VSV-G and cultured with the ligand. The intensity of GFP signal stays constant with or without dox treatment. Scale bar = 200  $\mu$ m.

recombination in T47D (eGFP+ reporter cells: 82.9%), HEK293FT (eGFP+ reporter cells: 87.2%), HepG2 (eGFP+ reporter cells: 78.8%), iPSC-Fibroblast (eGFP+ reporter cells: 55.1%), HUVEC (eGFP+ reporter cells: 94.8%), myoblast Cre-loxP reporter cells (eGFP+ reporter cells: 68.7%) as determined by microscopy- and flow cytometry analysis (Fig. 4C). Hence, Cre TOP-EVs can achieve highly effective functional delivery in various cell types.



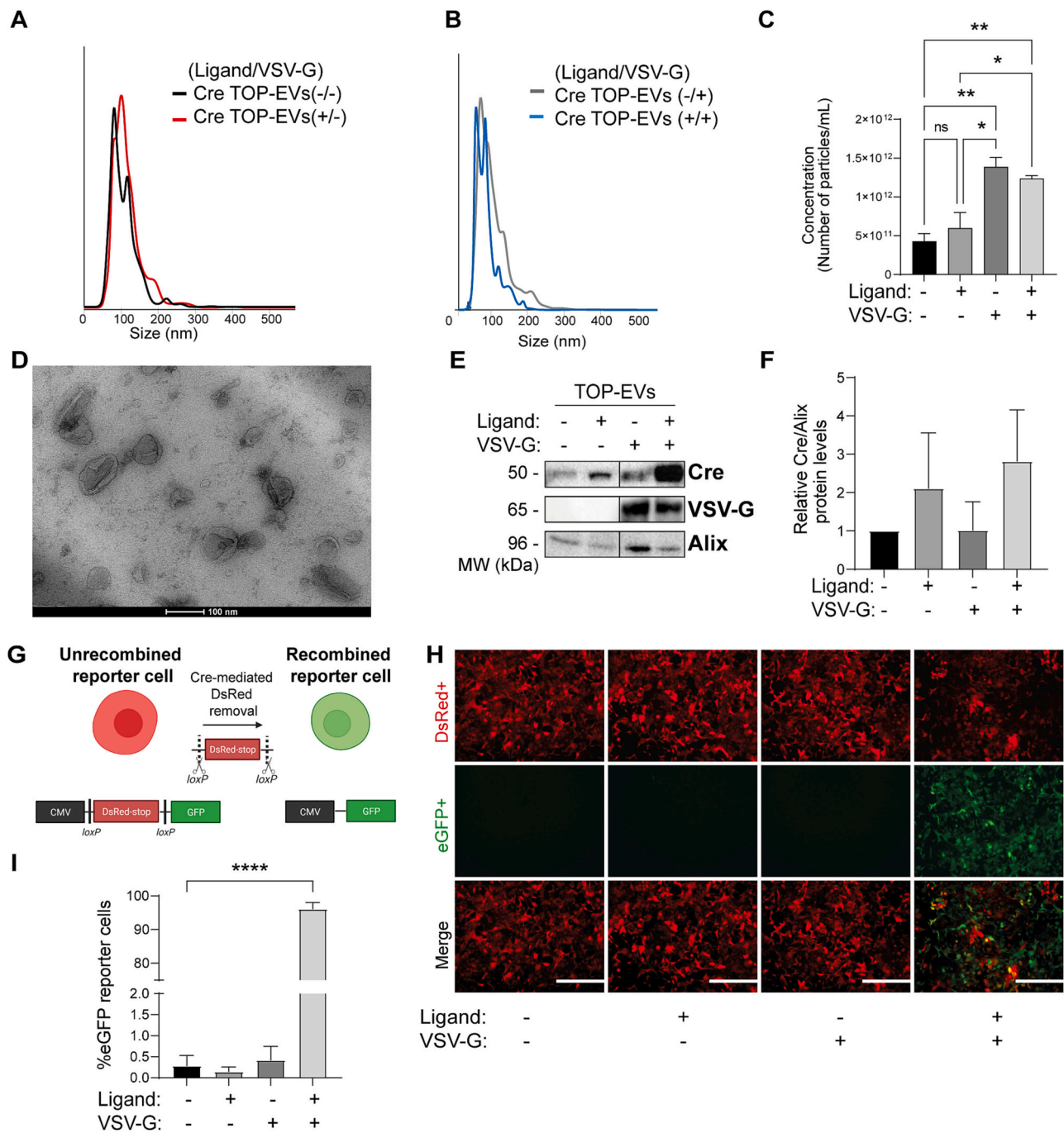


**Fig. 3.** TOP-EV characterization and mediated Cre delivery *in vitro* A, B. NTA analysis demonstrated that Cre TOP-EV with (+) or without (-) the ligand or VSV-G had a similar size distribution between 50 and 250 nm C. NTA analysis reveals that VSV-G increases the number of particles obtained after isolation by  $\pm 2.5$ -fold compared to donor cells without VSV-G. Representative data from six individual experiments. D. TEM images showed that Cre TOP-EVs (+/+; Ligand/VSV-G) had a 'cup-shaped' morphology. Scale bar = 100 nm E, F. Western blot analysis and quantification of Cre TOP-EVs obtained from donor cells co-transfected or co-cultured with (+) or without (-) VSV-G/Ligand. G. Schematic illustration of Cre reporter cell line where the introduction of Cre recombinase will target the loxP sites leading to DsRed+ removal and GFP+ expression in stoplight reporter cells. H, I. Fluorescence microscopy and flow cytometry analysis of Cre TOP-EVs (+/-; Ligand/VSV-G) administrated to T47D stoplight reporter cells. Scale bar = 400  $\mu$ m. Data expressed as mean  $\pm$  SEM of three individual experiments, analyzed using a one-way ANOVA with \* $p < 0.05$  and \*\* $p < 0.01$ .

### 3.5. Investigate TOP-EV uptake using Cre TOP-EV

We blocked known modulators of EV uptake and release in T47D stoplight reporter cells to explore Cre TOP-EVs' uptake and cargo release. Prior to Cre TOP-EV addition, we incubated inhibitors to block caveolae/lipid- (Nystatin), clathrin- (Chlorpromazine), and micropinocytosis (EIPA) dependent endocytosis. We included chloroquine, a

well-characterized agent capable of increasing the endosomal-pH, thereby inhibiting VSV-G induced-membrane fusion (Fig. 5A) [19–21]. Microscopy and flow cytometry analysis demonstrated that TOP-EV mediated Cre delivery was significantly reduced upon inhibition of clathrin-dependent endocytosis, micropinocytosis and endosomal acidification inhibition (Fig. 5B and C). These findings support that TOP-EV uptake in T47D stoplight reporter cells probably mediated *via* clathrin-

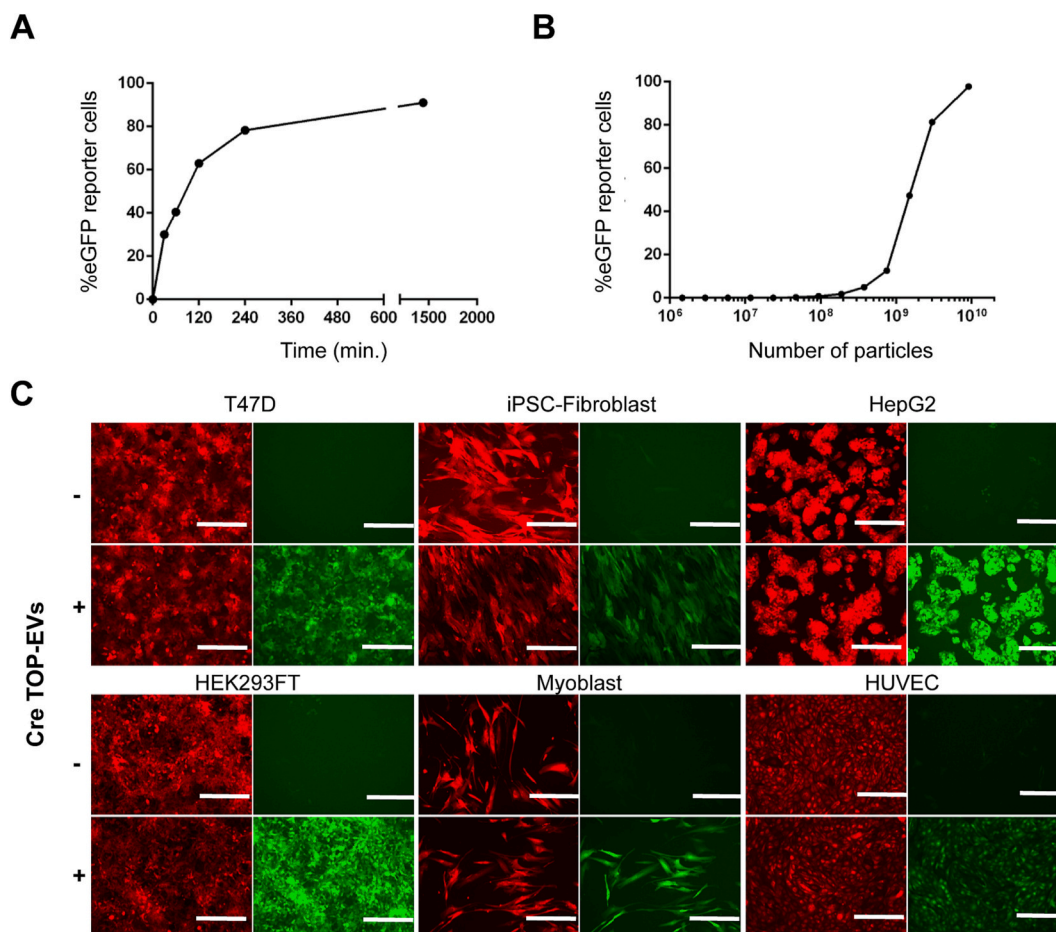


**Fig. 4.** Time-, dose- and cell type specific uptake of Cre TOP-EVs. A. Flow cytometry quantification of GFP+ reporter cells demonstrated a time and B. dose-dependent uptake of Cre TOP-EVs by T47D stoplight reporter cells. C. Microscopic analysis showed that Cre TOP-EV have broad cell uptake spectrum. Different cell types showed Cre mediated recombination after addition of  $10^{10}$  particles of Cre TOP-EVs. Scale bar = 400  $\mu$ m.

dependent endocytosis and macropinocytosis. In line with previous reports [22,23], we found VSV-G to be essential to the release of TOP-EV intraluminal cargo inside the recipient cells, which we showed occurs by endosomal escape through low pH-induced membrane fusion, as chloroquine significantly inhibits TOP-EVs mediated Cre-recombination in T47D stoplight reporter cells (Fig. 5B and C).

### 3.6. TOP-EV mediated CRISPR/Cas9 ribonucleoprotein delivery to mediate genome-editing

Various reports suggested that CRISPR/Cas9 RNPs could achieve efficient genome editing with reduced off-target effect due to the shorter lifetime compared to plasmid or mRNA vectors [24–26]. To further investigate the potential application of TOP-EVs, we created TOP-EVs loaded with CRISPR/Cas9 RNP by transient transfection of HEK293FT cells with Cas9-TOP construct, a sgRNA plasmid and with or without the VSV-G plasmid. Subsequently, Cas9 TOP-EVs were isolated from donor cells by differential ultracentrifugation upon culturing with or without the ligand. NTA demonstrated a similar size-distribution profile between Cas9 TOP-EV groups with an average diameter of  $106 \pm 2.32$  nm from Cas9 TOP-EV (+/-: Ligand/VSV-G) and  $113 \pm 2$  nm for Cas9 TOP-EV (+/+ : Ligand/VSV-G) (Fig. 6A and B), similar to our previous observations with Cre TOP-EVs (Fig. 3C, D). Furthermore, Cas9 TOP-EVs' without or with VSV-G had a mode size of  $81.8 \pm 4.5$  nm and  $80.6 \pm 3.3$  nm, respectively. The TEM image showed an EV-like morphology of Cas9 TOP-EV (+/+ : Ligand/VSV-G) (Fig. 6C). Western blot analysis showed that Cas9 TOP-EVs groups were negative for endoplasmic

reticulum marker calnexin and positive for EV marker proteins synthenin-1 and CD9 (Fig. S1). Furthermore, western blot analysis confirmed that TOP-EVs derived from donor cells co-transfected with VSV-G were 7.8-fold enriched with Cas9 protein normalized to TOP-EVs (-/-: Ligand/VSV-G). Moreover, donor cells co-transfected with VSV-G and cultured with the ligand produced TOP-EVs with a 9.5-fold higher Cas9 protein content relative to donor cells without both VSV-G and ligand (Fig. 6D and E). Once more, we confirmed that the ligand and VSV-G are needed for protein loading inside EVs.

To confirm the functional delivery of CRISPR/Cas9 RNP by TOP-EVs, we administrated Cas9 TOP-EVs to target cells with a CRISPR-operated stoplight system [13]. Upon CRISPR/Cas9 delivery in Cas9 stoplight reporter cells, on-target CRISPR/Cas9 RNP mediated non-homologous end-joining (NHEJ) of the linker region resulted in a + 1 nt or + 2 nt frameshift, eliciting permanent GFP expression in the Cas9 stoplight reporter (Fig. 6F) [13]. Fluorescence microscopy- and flow cytometric analysis confirmed that Cas9 TOP-EVs (-/+ : Ligand/VSV-G) and Cas9 TOP-EVs (+/+ : Ligand/VSV-G) mediated functional delivery of the CRISPR/Cas9 RNP complex inside Cas9 stoplight reporter cells (Fig. 6G and I). Flow cytometry analysis showed genome editing with an efficiency of  $11.6 \pm 1.5\%$  by Cas9-TOP-EV (-/+ : Ligand/VSV-G) and  $29.4 \pm 2.5\%$  by Cas9-TOP-EV (+/+ : Ligand/VSV-G) (Fig. 6G and I). The observed genome editing activity aligned with previous findings of VSV-G-enveloped EV delivery of Cas9 in human iPSCs [27]. Furthermore, we confirmed that Cas9 TOP-EVs (+/+ : Ligand/VSV-G) mediated CRISPR/Cas9 delivery leading to NHEJ events in Cas9 stoplight reporter cells by T7 endonuclease assay (Fig. 6I). Collectively, these observations showed



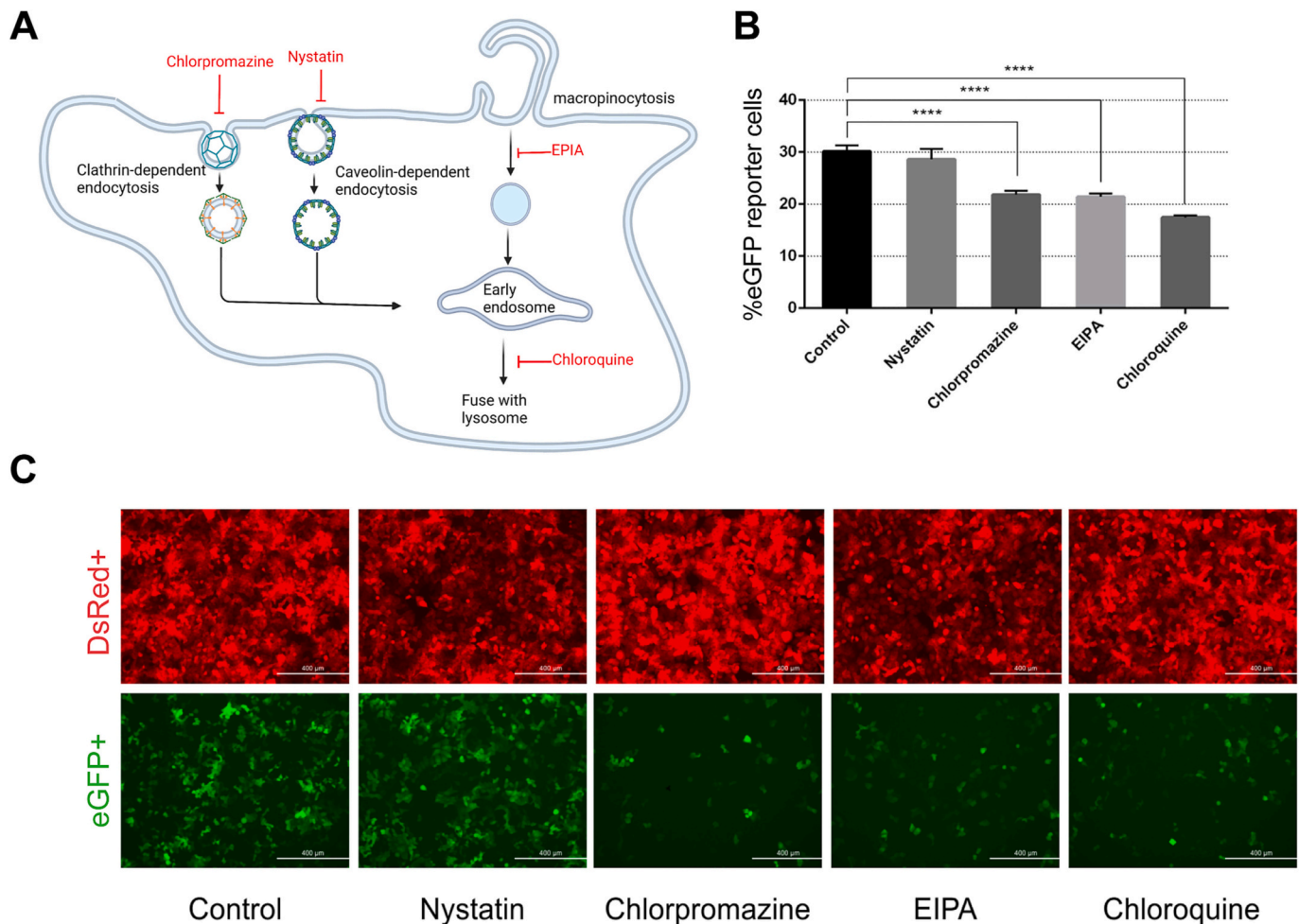


**Fig. 5.** TOP-EVs' uptake is mediated both by clathrin-dependent endocytosis and micropinocytosis. **A.** Schematic illustration of potential EV mediated uptake pathway and effect of endocytic pathway inhibitors. **B.** Flow cytometry analysis and in **C.** Microscopy analysis of Cre TOP-EV mediated recombination in T47D Cre stoplight reporter cells show TOP-EV uptake is unaffected by inhibition of caveolin-dependent endocytosis, but negatively affected when clathrin-dependent endocytosis and micropinocytosis is inhibited by chlorpromazine and EIPA, respectively. Furthermore, TOP-EV release of Cre is reduced by chloroquine which inhibits endosomal acidification. This observation hints VSV-G plays an important role in endosomal acidification to release the EVs cargo in the cytosol. Data expressed as mean  $\pm$  SEM of three individual experiments, analyzed using a one-way ANOVA with  $*p < 0,05$  and  $**p < 0,01$ . Scale bar = 400  $\mu$ m.

that TOP-EVs could successfully load and deliver CRISPR/Cas9 RNP to mediate effective genome editing in recipient cells.

### 3.7. TOP-EV mediated delivery of Cre to the liver

To study TOP-EV functional delivery of Cre recombinase protein *in vivo*, we administrated Cre TOP-EVs *via* tail-vein injection to Ai9 mice, with  $5 \times 10^{11}$  particles as dose being injected three times over the course of 3 days with 24 h intervals per injection. As negative control, Ai9 mice received PBS *via* intravenous (i.v.) injections. Successful intracellular delivery of Cre recombinase inside Ai9 mice induced a color-switch resulting in tdTomato+ cells (Fig. 7A). After 7 days since the initial Cre TOP-EV administration, the mice were sacrificed. Immunofluorescence histological analysis showed that TOP-EV mediate the functional delivery of Cre recombinase protein resulting in  $\pm 3.9\%$  tdTomato+Hoechst+ cells (Fig. 7B and C). Immunofluorescence histological analysis with hepatocyte nuclear factor 4 alpha (HNF4A) demonstrated TOP-EV could mediate the functional transfer of Cre recombinase protein into hepatocytes (Fig. 7D). These findings showed that TOP-EV can be applied for *in vivo* applications to facilitate the intracellular delivery of proteins to the liver following multiple i.v. injection.

## 4. Discussion

The development of biocompatible delivery platforms is pivotal since available synthetic drug delivery systems are burdened with low purification- and loading efficiency, immunogenic risk, and non-biocompatibility for protein delivery. EVs' natural role in involvement with biomolecule transfer, biocompatibility, and intrinsic targeting abilities make them an attractive delivery system for biotherapeutics. Loading protein into EVs is currently constrained by effective protein loading and poor endosomal escape in target cells. Therefore, we introduce the rapamycin-ortholog ligand inducible heterodimerization concept to achieve active endogenous protein loading inside EVs. By incorporating VSV-G on the EV membrane, we created TOP-EVs that efficiently load and mediate functional intracellular delivery for various target proteins *in vitro* and *in vivo*.

Previously, studies used light- and chemical induced protein interactions for protein loading into EVs. Yim et al. engineered optically reversible CRY2 to target proteins to interact with CIBN fused to the intraluminal domain of CD9 leading to EV-mediated Cre recombinase delivery *in vivo* after administration using their Cre:EXPLOR concept inside the ventrolateral part of the brain [28]. Alternatively, EVs protein loading through interactions of rapamycin or its analogs-inducible dimerization proteins FKBP and FRB variants have been employed

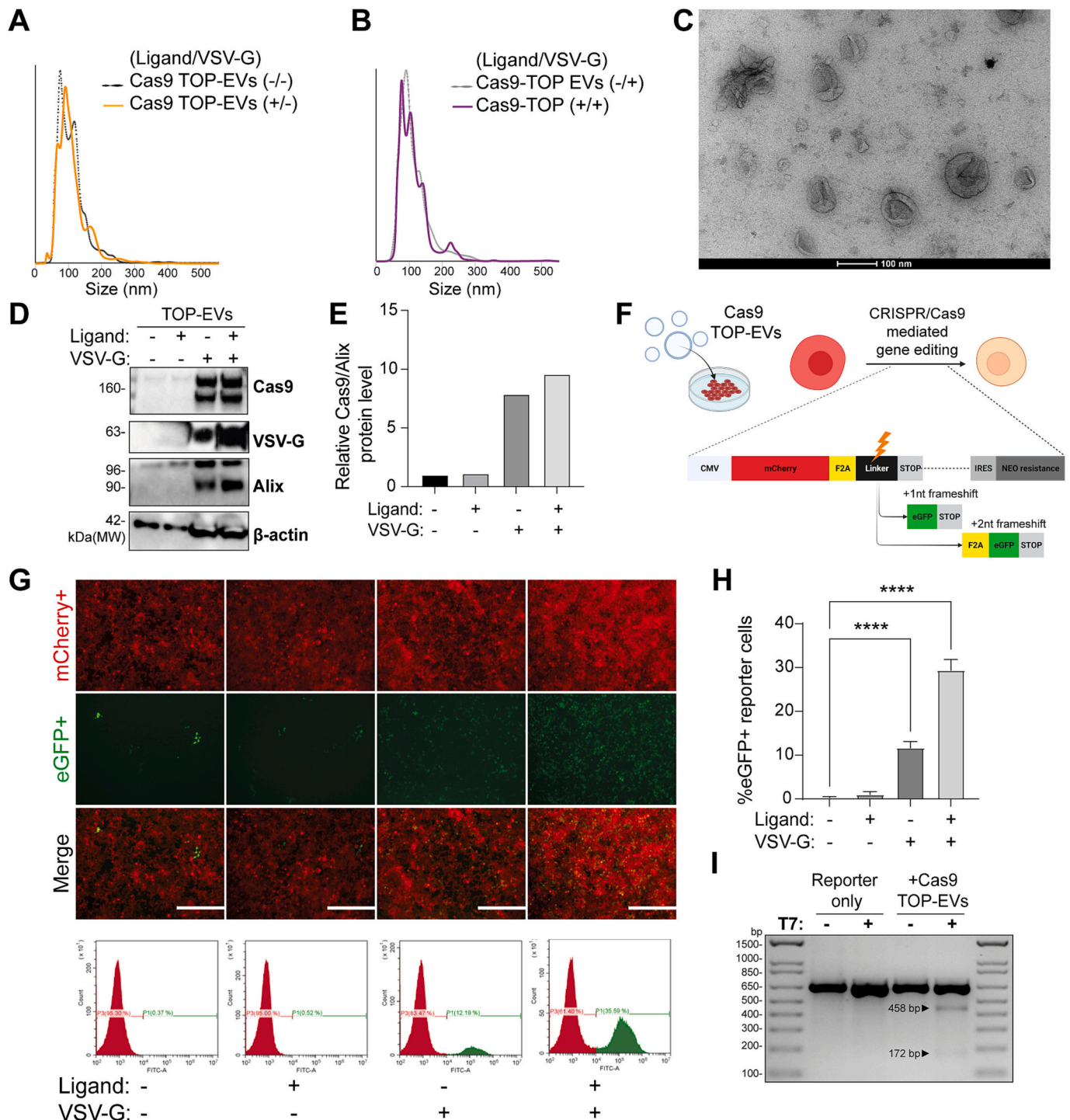


**Fig. 6. Characterization and TOP-EV mediated CRISPR/Cas9 RNP delivery *in vitro*** A, B. NTA analysis demonstrated that the Cas9 TOP-EV groups have a similar size distribution between 50 and 250 nm C. TEM image showed Cas9 TOP-EV (+/+; Ligand/VSV-G) has a circular morphology. Scale bar = 100 nm. D, E. Western blot analysis and quantification showed relative Cas9 protein levels inside EVs increased by 7.8-fold when VSV-G is introduced in the donor cells and by 9.5-fold with VSV-G co-transfection and culturing together with the ligand in donor cells. F. Schematic illustration of Cas9 stoplight reporter where successful CRISPR/Cas9 RNP delivery leads to a + 1 nt and + 2 nt frameshift resulting in GFP+ expression. G, H. Microscopy- and flow cytometric analysis of Cas9 TOP-EV mediated genome editing events in Cas9 stoplight reporter cells. Scale bar = 400 μm I. Validation of genome editing efficiency by T7 endonuclease assay. Data expressed as mean ± SEM of three individual experiments, analyzed using a one-way ANOVA with \**p* < 0,05 and \*\**p* < 0,01.

[18,26–28]. Together with VSV-G, FKBP-FRB engineered EVs have successfully mediated CRISPR/Cas9 delivery *in vitro* with an efficacy of ±30% in iPSC cells to inactivate GFP expression [27], similar to our findings in the Cas9 stoplight reporter cells. Furthermore, treatment with engineered EVs containing VSV-G and FKBP-FRB variants, relying on interaction with Gag, lowered proviral activity in HIV-infected cells

or successfully induced  $1.6 \pm 0.3\%$  genomic exon skipping efficiency in a Duchenne muscular disease mouse model [29] [30].

Compared to these previous studies, our study provides several novel aspects. First, prior published work did not demonstrate the role those individual component, *i.e.*, VSV-G and the rapamycin-orthologue, had on target protein loading inside TOP-EVs. Using GFP TOP-EV as an

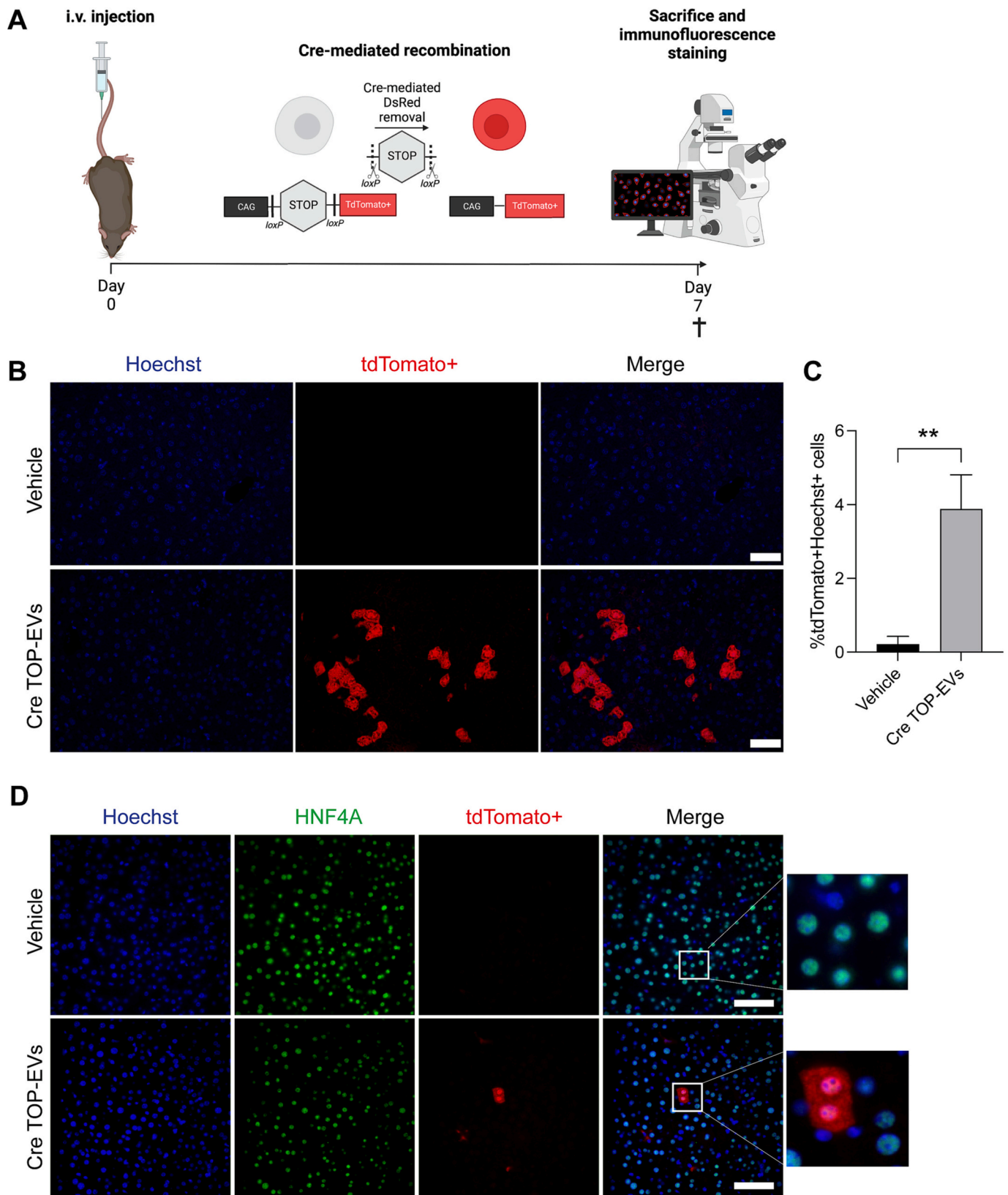


**Fig. 7. TOP-EV mediated delivery of Cre recombinase *in vivo*** A. Schematic illustration of study design administrating PBS (Vehicle) or multiple doses of Cre TOP-EVs in Ai9 mice. Successful intracellular delivery of Cre recombinase protein through TOP-EVs will result in a color-switch leading to tdTomato+ cells in Ai9 mice. B. Immunofluorescence images from liver sections of Ai9 mice that received i.v. injection of the vehicle or Cre TOP-EVs (+/+; Ligand/VSV-G) showed that TOP-EVs could mediate the functional transfer of Cre recombinase. Red = tdTomato, Blue = Hoechst. Scale bar = 50  $\mu$ m. C. Quantification of liver sections showed Cre TOP-EV administration resulted in  $\pm 3.9\%$  tdTomato+Hoechst+ cells. (D) Co-staining with hepatocyte nuclear factor 4 alpha (HNF4A) demonstrated that TOP-EVs facilitated the functional transfer of Cre recombinase to hepatocytes *in vivo*. Red = tdTomato, Green = HNF4A, Blue = Hoechst. Scale bar = 100  $\mu$ m. Data expressed as mean  $\pm$  SEM of three individual experiments, analyzed using a Welch's t-test with \* $p < 0.05$  and \*\* $p < 0.01$ .



example, we showed that >60% of TOP-EVs contained GFP and on average >90 GFP molecules were present in one TOP-EV (+/+; Ligand/VSV-G). Our study provides new insights demonstrating that rapamycin-induced dimerization together with VSV-G co-transfection were both important in promoting target protein loading and delivery through TOP-EVs. Conversely, target proteins were rarely loaded without donor cells co-transfected with VSV-G and cultured without the rapamycin-orthologue. Furthermore, we demonstrated that the FKBP12/FRB system could load CRISPR/Cas9 RNP within EVs. Through western blot analysis we found target proteins were loaded with different efficacies within EVs. Nonetheless, we showed that TOP-EVs could achieve functional delivery of Cre recombinase with unprecedented recombination efficiency and CRISPR/Cas9 RNP mediated genome-editing efficiency in their respective stoplight reporter systems. These findings showed that target proteins can be easily engineered inside the TOP plasmid and loaded inside TOP-EV *via* transient transfection. Second, for the first time in the field, we proved that TOP-EVs capacity to deliver intracellular proteins in recipient cells is not an artifact of plasmid contamination in the EV preparation from transiently transfected donor cells or *via* direct loading of plasmids into EVs. Third, using specific inhibitors in combination with Cre TOP-EV, we uncovered that TOP-EVs are taken up by clathrin-dependent uptake and macropinocytosis, and demonstrated that functional cargo delivery of our TOP-EVs is dependent on late endosomal acidification using the lysosomotropic agent chloroquine.

Finally, we demonstrated that TOP-EVs delivered Cre recombinase into the liver *in vivo*. In the past decade, approximately 18% of pre-clinical studies investigated EVs as drug delivery vehicle for protein or peptide-based entities [31]. These findings suggest that the delivery of peptides and proteins remains challenging. Our findings that multiple injections of TOP-EVs facilitated the functional intracellular delivery of Cre recombinase into the liver, including hepatocytes, could be very important in future study design. In conclusion, TOP-EVs are a versatile platform to promote endogenous protein loading and mediate functional intracellular protein delivery for *in vitro* and *in vivo* applications [25,27,28].

## 5. Limitation of the study

We observed that VSV-G was indispensable for TOP-EV to mediate functional delivery in target cells. Since VSV-G originated from a virus envelope protein, it should be tested to determine whether its immunogenicity may be detrimental during clinical application. Therefore, exploring the human homolog of VSV-G will be interesting in replacing VSV-G [33–35]. The use of VSV-G also demonstrated some cellular aspects for which we did not yet have an explanation, including the presence of a second Alix band *via* western blotting, an increase in EV particle number release, and changes in Alix expression levels.

Secondly, our data demonstrates TOP-EVs' efficient protein delivery capacity, but the possibility of mRNA cargo incorporation cannot be completely excluded. Previous work suggested that the occurrence of EV-mediated RNA transfer is extremely low. Moreover we anticipate that this will not be significantly problematic to interfere with practical applications of TOP-EVs [7]. Another limitation regarding cargo loading rate could not be determined with the current method for other payloads, such as Cre recombinase and Cas9 RNP.

Third, we only investigated TOP-EVs produced from a single cell source. Wiklander et al. found that EV biodistribution of EVs differs per cell source *in vivo* [32]. Future research into TOP-EV produced from different cell sources would shed more light on achieving (increased) targeted delivery into tissue, e.g. targeted delivery in the liver to reach hepatocytes more effectively than Kupffer cells.

Finally, we showed that TOP-EV could deliver Cre recombinase *in vivo* in various tissues through different administration routes, but the percentages of Cre-recombined tdTomato+ cells were still limited. Partly because the number of TOP-EVs administered compared with *in vitro* experiment was relatively low, considering the number of cells

in a whole animal. In this regard, strategies and technologies that can produce large quantity of EVs maybe helpful to solve this challenge. Also, Cre reporter animals provides an opportunity to study which cell type has taken up TOP-EV using single cell sequencing or immunohistochemistry study, which deserves an in-depth follow-up investigation in a future study.

## 6. Conclusion

The results presented in this study demonstrated that the TOP-EV platform provided the potential to realize intracellular protein delivery for many proteins. We foresee the TOP-EV as a versatile platform to mediate functional protein delivery for *in vitro* and *in vivo* applications, including genome editing.

## Funding

Funding for the present work was provided by the Project EVICARE [No. 725229] of the European Research Council (ERC) to J.P.G.S., co-funded by the Project SMARTCARE-II of the BioMedicalMaterials institute to J.P.G.S., the ZonMw-TAS program [No. 116002016] to J.P.G.S./Z.L., PPS grant [No. 2018B014] to J.P.G.S./Z.L./P.V./S.J., the Dutch Ministry of Economic Affairs, Agriculture and Innovation and the Netherlands CardioVascular Research Initiative (CVON): the Dutch Heart Foundation to J.P.G.S., Dutch Federations of University Medical Centers, the Netherlands Organization for Health Research and Development, and the Royal Netherlands Academy of Sciences.

## CRediT authorship contribution statement

**Nazma F. Ilahibaks:** Investigation, Data curation, Visualization, Formal analysis, Writing – original draft, Writing – review & editing. **Arif I. Ardisasmitta:** Investigation, Data curation, Visualization, Formal analysis, Writing – review & editing. **Songpu Xie:** Investigation, Data curation, Formal analysis. **Anders Gunnarsson:** Investigation, Data curation, Formal analysis. **Joseph Brealey:** Investigation, Data curation, Formal analysis. **Pieter Vader:** Supervision, Resources, Funding acquisition, Writing – review & editing. **Oliver G. de Jong:** Investigation. **Saskia de Jager:** Funding acquisition, Resources. **Niek Dekker:** Supervision, Resources, Funding acquisition. **Ben Peacock:** Supervision, Resources, Funding acquisition. **Raymond M. Schiffelers:** Funding acquisition, Resources. **Joost P.G. Sluijter:** Conceptualization, Supervision, Resources, Funding acquisition, Writing – review & editing. **Zhiyong Lei:** Conceptualization, Supervision, Funding acquisition, Writing – original draft, Writing – review & editing.

## Declaration of Competing Interest

P.V. serves on the scientific advisory board of Evox Therapeutics.

## Data availability

Data will be made available on request.

## Acknowledgments

The authors thank Peggy Karanatsiou, Qiangbing Yang, Peter Bokern, and Cor van Sein for their experimental support. The authors would like to thank Dr. Linglei Jiang for providing with Cre reporter cell line. The authors acknowledge the FACS facility as well as the infrastructure and support of Corlinda ten Brink and the Cell Microscopy Core of the Department of Cell Biology at the University Medical Center Utrecht in the Netherlands for the use of imaging equipment. Schematic illustrations have been created with [BioRender.com](https://BioRender.com).

## Appendix A. Supplementary data

Supplementary data to this article can be found online at <https://doi.org/10.1016/j.jconrel.2023.02.003>.

## References

- [1] S. Mitragotri, P.A. Burke, R. Langer, Overcoming the challenges in administering biopharmaceuticals: formulation and delivery strategies, *Nat. Rev. Drug Discov.* 13 (9) (2014) 655–672.
- [2] T. Wei, Q. Cheng, Y.-L. Min, E.N. Olson, D.J. Siegwart, Systemic nanoparticle delivery of CRISPR-Cas9 ribonucleoproteins for effective tissue specific genome editing, *Nat. Commun.* 11 (1) (2020) 1–12.
- [3] J. Xu, Z. Li, Q. Fan, J. Lv, Y. Li, Y. Cheng, Dynamic polymer Amphiphiles for efficient intracellular and in vivo protein delivery, *Adv. Mater.* (2021) 2104355.
- [4] B. Chatin, et al., Liposome-based formulation for intracellular delivery of functional proteins, *Mol. Therap.-Nucleic Acids* 4 (2015), e244.
- [5] N.-T. Chiou, K.M. Ansel, Improved Exosome Isolation by Sucrose Gradient Fractionation of Ultracentrifuged Crude Exosome Pellets, 2016.
- [6] C. Ettelaie, M.E.W. Collier, A. Maraveyas, R. Ettelaie, Characterization of physical properties of tissue factor-containing microvesicles and a comparison of ultracentrifuge-based recovery procedures, *J. Extracell. Vesicl.* 3 (1) (2014) 23592.
- [7] A. Zomer, et al., In vivo imaging reveals extracellular vesicle-mediated phenocopying of metastatic behavior, *Cell* 161 (5) (2015) 1046–1057.
- [8] O.G. de Jong, et al., Drug delivery with extracellular vesicles: from imagination to innovation, *Acc. Chem. Res.* 52 (7) (2019) 1761–1770.
- [9] D.E. Murphy, O.G. de Jong, M.J.W. Evers, M. Nurazizah, R.M. Schiffelers, P. Vader, Natural or synthetic RNA delivery: a stoichiometric comparison of extracellular vesicles and synthetic nanoparticles, *Nano Lett.* 21 (4) (2021) 1888–1895.
- [10] M.J. Haney, et al., Exosomes as drug delivery vehicles for Parkinson's disease therapy, *J. Control. Release* 207 (2015) 18–30.
- [11] S.A.A. Kooijmans, et al., Electroporation-induced siRNA precipitation obscures the efficiency of siRNA loading into extracellular vesicles, *J. Control. Release* 172 (1) (2013) 229–238.
- [12] U. Sterzenbach, U. Putz, L.-H. Low, J. Silke, S.-S. Tan, J. Howitt, Engineered exosomes as vehicles for biologically active proteins, *Mol. Ther.* 25 (6) (2017) 1269–1278.
- [13] O.G. de Jong, et al., Publisher correction: a CRISPR-Cas9-based reporter system for single-cell detection of extracellular vesicle-mediated functional transfer of RNA, *Nat. Commun.* 11 (1) (2020) 1.
- [14] L.A. Banaszynski, C.W. Liu, T.J. Wandless, Characterization of the FKBP $\odot$  rapamycin $\odot$  FRB ternary complex, *J. Am. Chem. Soc.* 127 (13) (2005) 4715–4721.
- [15] A.M. Silva, et al., Quantification of protein cargo loading into engineered extracellular vesicles at single-vesicle and single-molecule resolution, *J. Extracell. Vesicl.* 10 (10) (2021), e12130.
- [16] R. Lees, et al., Single extracellular vesicle transmembrane protein characterization by nano-flow cytometry, *J. Vis. Exp.* 185 (2022) 2022.
- [17] P.-E. Mangeot, et al., Protein transfer into human cells by VSV-G-induced Nanovesicles, *Mol. Ther.* 19 (9) (2011) 1656–1666, <https://doi.org/10.1038/mt.2011.138>.
- [18] A. Zomer, S.C. Steenbeek, C. Maynard, J. van Rheenen, Studying extracellular vesicle transfer by a Cre-loxP method, *Nat. Protoc.* 11 (1) (2015) 87–101, <https://doi.org/10.1038/nprot.2015.138>.
- [19] B.J. Dille, T.C. Johnson, Inhibition of vesicular stomatitis virus glycoprotein expression by chloroquine, *J. Gen. Virol.* 62 (1) (1982) 91–103.
- [20] N. Heath, et al., Endosomal escape enhancing compounds facilitate functional delivery of extracellular vesicle cargo, *Nanomedicine* 14 (21) (2019) 2799–2814.
- [21] B.L. Fredericksen, B.L. Wei, J. Yao, T. Luo, J.V. Garcia, Inhibition of endosomal/lysosomal degradation increases the infectivity of human immunodeficiency virus, *J. Virol.* 76 (22) (2002) 11440–11446.
- [22] M. Somiya, S. Kuroda, Real-time luminescence assay for cytoplasmic cargo delivery of extracellular vesicles, *Anal. Chem.* 93 (13) (2021) 5612–5620.
- [23] R.Z. Florkiewicz, J.K. Rose, A cell line expressing vesicular stomatitis virus glycoprotein fuses at low pH, *Science* (1979) 225 (4663) (1984) 721–723.
- [24] G.A. Newby, et al., Base editing of haematopoietic stem cells rescues sickle cell disease in mice, *Nature* (2021) 1–8.
- [25] J.L. Doman, A. Raguram, G.A. Newby, D.R. Liu, Evaluation and minimization of Cas9-independent off-target DNA editing by cytosine base editors, *Nat. Biotechnol.* 38 (5) (2020) 620–628.
- [26] S. Banskota, et al., Engineered virus-like particles for efficient in vivo delivery of therapeutic proteins, *Cell* (2022).185(2): 250–265. e16.
- [27] C. Montagna, et al., VSV-G-enveloped vesicles for traceless delivery of CRISPR-Cas9, *Mol. Therap.-Nucleic Acids* 12 (2018) 453–462.
- [28] N. Yim, et al., Exosome engineering for efficient intracellular delivery of soluble proteins using optically reversible protein-protein interaction module, *Nat. Commun.* 7 (2016) 1–9, <https://doi.org/10.1038/ncomms12277>.
- [29] L.A. Campbell, L.M. Coke, C.T. Richie, L.V. Fortuno, A.Y. Park, B.K. Harvey, Gsicle-mediated delivery of CRISPR/Cas9 ribonucleoprotein complex for inactivating the HIV provirus, *Mol. Ther.* 27 (1) (2018) 1–13, <https://doi.org/10.1016/j.ymthe.2018.10.002>.
- [30] P. Gee, et al., Extracellular nanovesicles for packaging of CRISPR-Cas9 protein and sgRNA to induce therapeutic exon skipping, *Nat. Commun.* 11 (1) (2020) 1–18.
- [31] P.E.M. de Castilla, et al., Extracellular vesicles as a drug delivery system: a systematic review of preclinical studies, *Adv. Drug Deliv. Rev.* 175 (2021), 113801.
- [32] O.P.B. Wiklander, et al., Extracellular vesicle in vivo biodistribution is determined by cell source, route of administration and targeting, *J. Extracell. Vesicl.* 4 (2015) 1–13, <https://doi.org/10.3402/JEV.V4.26316>.
- [33] B. Uygur, K. Melikov, A. Arakelyan, L.B. Margolis, L.V. Chernomordik, Syncytin 1 dependent horizontal transfer of marker genes from retrovirally transduced cells, *Sci. Rep.* 9 (1) (2019) 17637, <https://doi.org/10.1038/s41598-019-54178-y>.
- [34] N. Grandi, E. Tramontano, HERV envelope proteins: physiological role and pathogenic potential in cancer and autoimmunity, *Front. Microbiol.* 9 (2018) 462.
- [35] M. Segel, et al., Mammalian retrovirus-like protein PEG10 packages its own mRNA and can be pseudotyped for mRNA delivery, *Science* (1979) 373 (6557) (2021) 882–889.